Plastic Relaxation of Thermoelastic Stress in Aluminum/Ceramic Composites

C.T. KIM, J.K. LEE, and M.R. PLICHTA

The dislocation generation due to a thermoelastic stress in 2024 Al/ceramic (SiC or TiC) composites was studied using transmission electron microscopy (TEM). Composites containing different ceramic particulates, ceramic volume fraction, and particle size were investigated. Dislocation density profiles were measured as a function of the distance from an Al/ceramic interface and compared with those calculated from an elastoplasticity model which accounts for the volume fraction of the ceramic particles. The intensity of dislocation generation showed a strong particle size dependence: as the ceramic particle size became of the order of a micron, the intensity of dislocation generation increased significantly. With an increase in the volume fraction of the ceramic particles, the dislocation density also increased, and the dislocation structure became a more tangled arrangement. If heat dissipation was taken into account as part of the plastic work, the predicted dislocation densities of the elastoplasticity model were found to be in reasonable agreement with the measured dislocation densities of 10^9 to 10^{10} cm^{-2}.

I. INTRODUCTION

PLASTIC relaxation of the elastic stress and strain energy associated with both thermal misfitting inclusions and lattice mismatching precipitates has been long recognized. Examples of dislocation generation due to a thermal misfit in the vicinity of an inclusion include the observations by Vogelsang *et al.*[1] and Arsenault and Fisher[2] on dislocation generation in the aluminum alloy matrix surrounding SiC whiskers or platelets and the finding by Chawla and Metzger[3] of higher dislocation densities at the Cu/W composite interface. The mechanical properties of the composite, therefore, should be affected by the magnitude and extent of the dislocation generation that takes place in the soft matrix around hard particles as a result of the relaxation of thermal misfit stress in the interface region.

The plastic deformation of a misfitting inclusion in an infinite matrix has been analyzed *via* a continuum mechanics model[4,5,6] as well as a dislocation loop-punching model.[7,8] Lee *et al.*[4] were able to deduce a particle size-dependent yield stress from the Ashby-Johnson model[8] for the nucleation of a dislocation from a particle/matrix interface. They showed two effective yield stresses which depend upon the coherency of the particle/matrix interface. One is essentially independent of the particle size and equal to the theoretical yield strength, $\mu/2\pi$, where μ is the matrix shear modulus. The other effective yield stress applies to incoherent particles and is a strong function of particle size. When the particle is very small, say of the order of 10 to 20 nm, this stress approaches the theoretical yield strength. When the particle size becomes of the order of a micron, the effective yield stress approaches an average (low-temperature) macroscopic yield stress.

Since in metal/matrix ceramic composites (MMC's) the particle/matrix interface is considered to be incoherent, it is expected that the dislocation generation due to a thermal expansion mismatch would depend strongly on the size of the ceramic particles in MMC's. Although the continuum mechanics and dislocation loop-punching models appear to yield fairly reasonable predictions for the experimentally observed dislocation generation, to date there have been no systematic experimental studies on the particle size-dependent dislocation generation. Additionally, the previous theoretical models were based on a single inclusion embedded in an infinite matrix, thus neglecting the effect of a multiparticle distribution. Therefore, a theoretical model for the plastic relaxation is desired to account for the volume fraction of ceramic particles in composites.

The purpose of this work was to examine experimentally the dislocation generation due to the different thermal contractions in Al/ceramic (SiC or TiC) composites. Materials containing different ceramic particulates, volume fractions of the ceramic, and sizes of ceramic were investigated. An effort was also made to develop a theoretical model for the plastic relaxation around a spherical particle, which incorporates the volume fraction of ceramic particles.

II. THEORY

For mathematical simplicity, we assume that all of the ceramic particles are of spherical shape with radius a, and further, that a given particle is surrounded by uniformly distributed neighboring particles. This assumption allows us to use spherical coordinates whose origin is at the center of a ceramic particle with radial symmetry, as shown schematically in Figure 1. In the manner of Lee *et al.*,[4] perfect plastic behavior is assumed for the matrix phase, and the crystallographic nature of plastic flow is neglected. However, the present model accounts for the volume fraction of ceramic particles. Thus, the matrix is considered to yield under the condition of a constant yield stress, and the yielding is considered independent of the stress axis. We shall first obtain the stress and strain associated with a misfitting spherical hard particle in the absence of plastic relaxation, *i.e.*,

C.T. KIM, Graduate Student, J.K. LEE, Professor, and M.R. PLICHTA, Associate Professor, are with the Department of Metallurgical Engineering, Michigan Technological University, Houghton, MI 49931.

Manuscript submitted June 7, 1989.

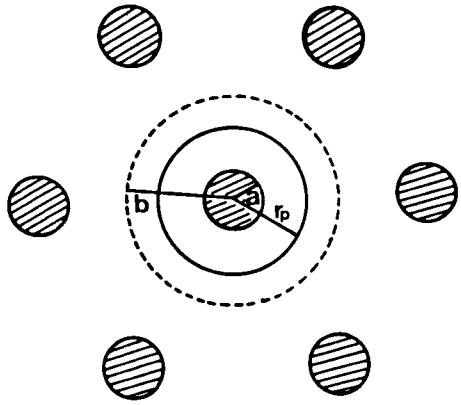

Fig. 1—A schematic diagram for an idealized ceramic configuration and plastic zone.

under purely elastic conditions. Then, employing the foregoing assumptions and continuum plasticity theory,[9,10] the solution for the elastoplastic deformation is determined when plastic relaxation takes place in the matrix.

A. *Pure Elastic State*

Consider a thick hollow sphere whose internal surface of radius a is subjected to a pressure, P_1, by the thermal misfitting ceramic particle and whose external surface of radius b is subjected to a pressure, P_2, by the surrounding ceramic particles, as shown in Figure 1. Because of the radial symmetry approximation, the tangential displacements, as well as the shear stresses and shear strains, are all zero, and the radial displacement, u, is a function of the radial distance, r. Further, the equilibrium equations in the absence of body forces reduce to

$$\frac{d\sigma_r}{dr} + \frac{2(\sigma_r - \sigma_\theta)}{r} = 0 \qquad [1]$$

where σ_r and σ_θ are radial and tangential stress components, respectively. The strains are related to the radial displacement, u, by

$$e_r = \frac{du}{dr}, \qquad e_\theta = \frac{u}{r} \qquad [2]$$

For the third diagonal components, $\sigma_\phi = \sigma_\theta$ and $e_\phi = e_\theta$ are implicitly assumed. Hooke's law provides

$$e_r = \frac{1}{E}(\sigma_r - 2\nu\sigma_\theta) + \alpha \cdot \Delta T \qquad [3a]$$

$$e_\theta = \frac{1}{E}[-\nu\sigma_r + (1 - \nu)\sigma_\theta] + \alpha \cdot \Delta T \qquad [3b]$$

where α is the thermal expansion coefficient and ΔT is the difference between the temperature of interest (room temperature in this study) and the solutionizing temperature for the composites. We note that with the above definition for the strain, the reference state is the one at the solutionizing temperature. The strain compatibility relationship is

$$e_r = e_\theta + \frac{r\, de_\theta}{dr} \qquad [4]$$

Substitution of the stress-strain Eq. [3] into Eq. [4] yields

$$\frac{1}{2}\frac{d^2}{dr^2}(r^2\sigma_r) - \sigma_r = 0 \qquad [5]$$

After integration, the radial stress is given by

$$\sigma_r = A - \frac{B}{r^3} \qquad [6]$$

and from Eq. [1] the tangential stress is

$$\sigma_\theta = A + \frac{B}{2r^3} \qquad [7]$$

The boundary conditions appropriate for small ceramic volume fractions are

$$\sigma_r(r = a) = -P_1 \qquad [8a]$$

$$\sigma_r(r = b) = -P_2 \qquad [8b]$$

$$u(r = b) = \alpha_m \cdot \Delta T \cdot b \qquad [8c]$$

Equation [8c] represents the displacement at the midpoint between two neighboring particles. Since the stress mode is critically influenced by the boundary conditions, their validity (especially Eqs. [8b] and [8c]) will be further discussed in Section V.

Substitution of Eqs. [8a] and [8b] into Eqs. [6] and [7] leads to the stresses in terms of the contact pressures, P_1 and P_2, as

$$\sigma_r = \frac{P_1a^3 - P_2b^3}{b^3 - a^3} - \frac{a^3b^3(P_1 - P_2)}{(b^3 - a^3)r^3} \qquad [9a]$$

$$\sigma_\theta = \frac{P_1a^3 - P_2b^3}{b^3 - a^3} + \frac{a^3b^3(P_1 - P_2)}{2(b^3 - a^3)r^3} \qquad [9b]$$

Substituting Eqs. [9a] and [9b] into Eq. [3b] yields displacement as

$$u = \frac{(1 + \nu_m)a^3b^3(P_1 - P_2)}{2E_m(b^3 - a^3)r^2} + \left(\frac{(1 - 2\nu_m)(P_1a^3 - P_2b^3)}{E_m(b^3 - a^3)} + \alpha_m \cdot \Delta T\right)r \qquad [10]$$

Utilizing the boundary condition of Eq. [8c], P_2 is given by

$$P_2 = \frac{3a^3(1 - \nu_m)P_1}{a^3 + 2b^3 + \nu_m(a^3 - 4b^3)} \qquad [11]$$

Further substitution of Eq. [11] into Eqs. [9a] and [9b] yields

$$\sigma_r = \frac{-P_1a^3(1 + \nu_m)}{a^3 + 2b^3 + \nu_m(a^3 - 4b^3)} - \frac{2a^3b^3(1 - 2\nu_m)P_1}{a^3 + 2b^3 + \nu_m(a^3 - 4b^3)}\left(\frac{1}{r^3}\right) \qquad [12a]$$

$$\sigma_\theta = \frac{-P_1a^3(1 + \nu_m)}{a^3 + 2b^3 + \nu_m(a^3 - 4b^3)} + \frac{a^3b^3(1 - 2\nu_m)P_1}{a^3 + 2b^3 + \nu_m(a^3 - 4b^3)}\left(\frac{1}{r^3}\right) \qquad [12b]$$

Since both the constrained displacement and the traction must be continuous at the ceramic/matrix interface, $r = a$, we first obtain, by setting $e_\theta^c = e_\theta^m$ from Eq. [3b],

$$\alpha_c \cdot \Delta T + \frac{1}{E_c}[-\nu_c \sigma_r^c + (1 - \nu_c)\sigma_\theta^c] = \alpha_m \cdot \Delta T + \frac{1}{E_m}[-\nu_m \sigma_r^m + (1 - \nu_m)\sigma_\theta^m] \quad [13]$$

and by substituting $\sigma_r^c = \sigma_\theta^c = -P_1 = \sigma_r^m$ into Eq. [13], we get

$$\sigma_\theta = \frac{P_1[b^3 - a^3 - \nu_m(a^3 + 2b^3)]}{a^3 + 2b^3 + \nu_m(a^3 - 4b^3)} \quad \text{at } r = a$$

Solving Eq. [13] for P_1 yields

$$P_1 = \frac{-(\alpha_m - \alpha_c)\Delta T}{\frac{1}{E_m}\left[\nu_m + (1 - \nu_m)\frac{b^3 - a^3 - \nu_m(a^3 + 2b^3)}{a^3 + 2b^3 + \nu_m(a^3 - 4b^3)}\right] + \frac{1 - 2\nu_c}{E_c}} \quad [14]$$

Substitution of Eq. [14] into Eqs. [12a] and [12b] provides the elastic stress components for the matrix phase. Note that if there is no difference between the two thermal expansion coefficients, α_m and α_c, no elastic stress arises in the composite.

B. *Plastic Relaxation*

When an effective elastic stress exceeds the yield stress of a metallic crystal, the crystal will undergo plastic deformation rather than remain in a purely elastic state. Since the stress state within the spherical ceramic is hydrostatic, the ceramic is considered to remain in a purely elastic state. Plastic deformation, therefore, can be considered to occur only in the matrix adjacent to the ceramic, as schematically shown in Figure 1, where r_p is the radius of the plastic zone.

For mathematical simplicity, two additional assumptions are made for the model on the plastic behavior of the matrix. First, we assume that the flow stress-strain behavior of the matrix phase is independent of the strain rate and also of the stress orientation. Second, we neglect strain hardening, so that the matrix phase is taken to be a perfectly plastic material whose flow stress-strain curve is horizontal at the yield stress, σ_y. We adopt the von Mises yielding criterion,[11] namely, that yielding occurs when an equivalent stress, σ_e, exceeds the yield stress, σ_y, where σ_e is given by

$$\sigma_e = \frac{1}{\sqrt{2}}[(\sigma_r - \sigma_\theta)^2 + (\sigma_\theta - \sigma_\phi)^2 + (\sigma_\phi - \sigma_r)^2]^{1/2} \quad [15]$$

Substitution of Eq. [12] into Eq. [15] yields

$$\sigma_e = \frac{3a^3b^3(1 - 2\nu_m)P_1}{a^3 + 2b^3 + \nu_m(a^3 - 4b^3)}\left(\frac{1}{r^3}\right) \quad [16]$$

The equilibrium equation (Eq. [1]) for the plastic shell, in conjunction with the yield condition, $\sigma_\theta - \sigma_r = \sigma_y$, becomes

$$\frac{d\sigma_r}{dr} - \frac{2\sigma_y}{r} = 0 \quad [17]$$

Integrating Eq. [17] and using the boundary condition $\sigma_r = -P_1$ at $r = a$,

$$\sigma_r = 2\sigma_y \ln (r/a) - P_1 \quad [18a]$$

$$\sigma_\theta = \sigma_y[1 + 2 \ln (r/a)] - P_1; \qquad a \leqq r < r_p \quad [18b]$$

Yielding occurs when $\sigma_e = \sigma_y$ at $r = r_p$. Thus, replacing r_p for a and P_p for P_1 in Eq. [16], we obtain

$$\frac{3r_p^3b^3(1 - 2\nu_m)P_p}{r_p^3 + 2b^3 + \nu_m(r_p^3 - 4b^3)}\left(\frac{1}{r_p^3}\right) = \sigma_y \quad [19]$$

From Eq. [19],

$$P_p = \frac{\sigma_y[r_p^3 + 2b^3 + \nu_m(r_p^3 - 4b^3)]}{3b^3(1 - 2\nu_m)} \quad [20]$$

By substituting P_p of Eq. [20] for P_1 and r_p for a in Eqs. [12a] and [12b], the stress components in the purely elastic region of the matrix are obtained as

$$\sigma_r = \frac{-(1 + \nu_m)\sigma_y}{3(1 - 2\nu_m)}(r_p/b)^3 - \frac{2\sigma_y}{3}(r_p/r)^3 \quad [21a]$$

$$\sigma_\theta = \frac{-(1 + \nu_m)\sigma_y}{3(1 - 2\nu_m)}(r_p/b)^3 + \frac{\sigma_y}{3}(r_p/r)^3; \qquad r_p \leqq r \leq b \quad [21b]$$

Since the radial stress must be continuous at the plastic front, the plastic zone radius, r_p, is obtained by equating Eqs. [18a] and [21a] at $r = r_p$.

$$2\sigma_y \ln (r_p/a) - P_1 = \frac{-(1 + \nu_m)\sigma_y}{3(1 - 2\nu_m)}(r_p/b)^3 - \frac{2\sigma_y}{3} \quad [22]$$

By applying the relationship between the displacement and the radial stress in the purely elastic state given in Eqs. [2] and [3b] to the radial stress given in Eq. [21a], the displacement outside the plastic zone is found to be

$$u = \frac{(1 + \nu_m)\sigma_y r_p^3}{3E_m r^2} - \left(\frac{(1 + \nu_m)\sigma_y}{3E_m}(r_p/b)^3 - \alpha_m \cdot \Delta T\right)r \quad [23]$$

Substituting Eq. [23] into Eq. [2],

$$e_r = \frac{-(1 + \nu_m)\sigma_y r_p^3}{3E_m}\left(\frac{2}{r^3} + \frac{1}{b^3}\right) + \alpha_m \cdot \Delta T \quad [24a]$$

$$e_\theta = \frac{(1 + \nu_m)\sigma_y r_p^3}{3E_m}\left(\frac{1}{r^3} - \frac{1}{b^3}\right) + \alpha_m \cdot \Delta T; \qquad r_p \leqq r \leq b \quad [24b]$$

Within the plastic zone, the strains are the sum of the plastic and elastic strains. Since the elastic strains are related to stresses by Hooke's law, we can write

$$e_r = \frac{du}{dr} = \frac{1}{E_m}(\sigma_r - 2\nu_m\sigma_\theta) + \alpha_m \cdot \Delta T + e_r^p \quad [25]$$

$$e_\theta = \frac{u}{r} = \frac{1}{E_m}[-\nu_m\sigma_r + (1 - \nu_m)\sigma_\theta] + \alpha_m \cdot \Delta T + e_\theta^p; \qquad a \le r < r_p \quad [26]$$

Here, e_r^p and e_θ^p denote plastic strain components in the plastic zone. In order to obtain the displacement, u, in the plastic zone, we use the incompressibility condition for plastic strains, $e_r^p + 2e_\theta^p = 0$. Multiplying Eq. [26] by 2, adding the result to Eq. [25], and using Eqs. [18a] and [18b] yields

$$\frac{du}{dr} + \frac{2u}{r} = \frac{2\sigma_y(1 - 2\nu_m)}{E_m}[1 + 3\ln(r/a)] - \frac{3(1 - 2\nu_m)P_1}{E_m} + 3\alpha_m \cdot \Delta T \quad [27]$$

for which the general solution is

$$u = \frac{2(1 - 2\nu_m)\sigma_y}{E_m} r \ln(r/a) - \left[\frac{(1 - 2\nu_m)P_1}{E_m} - \alpha_m \cdot \Delta T\right] r + \frac{C}{r^2}; \qquad a \le r < r_p \quad [28]$$

where C is an integration constant. Equating Eq. [23] to Eq. [28] with $r = r_p$ and rearranging the result with Eq. [22] furnishes an expression for u in Eq. [28]:

$$u = \frac{2(1 - 2\nu_m)\sigma_y}{E_m} r \ln(r/a) - \left[\frac{(1 - 2\nu_m)P_1}{E_m} - \alpha_m \cdot \Delta T\right] r + \frac{(1 - \nu_m)\sigma_y}{E_m}\frac{r_p^3}{r^2}; \qquad a \le r < r_p \quad [29]$$

From Eqs. [25], [26], and [29], the strains in the plastic zone are given as

$$e_r = \frac{2(1 - 2\nu_m)\sigma_y}{E_m}[\ln(r/a) + 1] + \alpha_m \cdot \Delta T - \frac{(1 - 2\nu_m)P_1}{E_m} - \frac{2(1 - \nu_m)\sigma_y}{E_m}(r_p/r)^3 \quad [30a]$$

$$e_\theta = \frac{2(1 - 2\nu_m)\sigma_y}{E_m}\ln(r/a) + \alpha_m \cdot \Delta T - \frac{(1 - 2\nu_m)P_1}{E_m} + \frac{(1 - \nu_m)\sigma_y}{E_m}(r_p/r)^3 \quad [30b]$$

$$e_r^p = -2e_\theta^p = \frac{2(1 - \nu_m)\sigma_y}{E_m}[1 - (r_p/r)^3]; \qquad a \le r < r_p \quad [30c]$$

In order to determine the equilibrium pressure, P_1, upon plastic relaxation, use is made of the continuity condition for both the (constrained) displacement and the traction at the ceramic/matrix interface. From Eq. [3b], for the tangential elastic strain within the ceramic, we have

$$e_\theta = \frac{u}{r} = \frac{1}{E_c}[-\nu_c\sigma_r^c + (1 - \nu_c)\sigma_\theta^c] + \alpha_c \cdot \Delta T = \frac{-P_1(1 - 2\nu_c)}{E_c} + \alpha_c \cdot \Delta T \quad [31]$$

The displacement within the ceramic is then given by

$$u = \left[\frac{-P_1(1 - 2\nu_c)}{E_c} + \alpha_c \cdot \Delta T\right] r; \qquad 0 \leqq r \leqq a \quad [32]$$

Finally, equating Eq. [29] and Eq. [32] at $r = a$ provides a solution for P_1:

$$P_1 = \frac{(\alpha_m - \alpha_c)\Delta T + \frac{(1 - \nu_m)\sigma_y}{E_m}(r_p/a)^3}{\frac{1 - 2\nu_m}{E_m} - \frac{1 - 2\nu_c}{E_c}} \quad [33]$$

Substituting Eq. [33] into Eq. [22] for P_1 gives an equation for r_p which can be solved for a given set of material parameters, E, ν, σ_y, α, and ΔT. If the materials are elastically homogeneous, *i.e.*, $E_m = E_c$ and $\nu_m = \nu_c$, equating Eq. [29] to Eq. [32] with $r = a$ yields directly

$$r_p = a[(\alpha_c - \alpha_m)\,\Delta T\, E_m/(1 - \nu_m)\sigma_y]^{1/3} \quad [34]$$

Further substitution of Eq. [34] into Eq. [22] yields P_1 for an elastically homogeneous case.

C. *Strain Energy*

The elastic strain energy inside the spherical ceramic, ω_c, per unit volume of the ceramic is given as

$$\omega_c = \frac{1}{2}[3\sigma_r(e_r - \alpha_c \cdot \Delta T)] = \frac{3P_1^2(1 - 2\nu_c)}{2E_c} \quad [35]$$

where P_1 is given in Eq. [33].

The total work consumed in the plastic zone is the sum of the plastic strain energy and the elastic strain energy. The plastic work per unit volume of an element located at distance, r, is, by definition[10]

$$\omega^p(r) = \int d\omega^p(r) = \int \sigma_{ij}\, de_{ij}^p = \int_0^{e_r^p} \sigma_r\, de_r^p + \int_0^{e_\theta^p} 2\sigma_\theta\, de_\theta^p \quad [36]$$

where the usual tensor suffix notation is used in the first equation. From the incompressibility condition, $e_r^p + 2e_\theta^p = 0$ for the plastic strains, we have $de_r^p = -2de_\theta^p$. Substituting this relationship into Eq. [36] and noting that $\sigma_r - \sigma_\theta = -\sigma_y$ = a constant, we obtain

$$\omega^p(r) = \int_0^{e_r^p} (\sigma_r - \sigma_\theta)\, de_r^p = -\sigma_y e_r^p = \frac{2(1 - 2\nu_m)\sigma_y^2}{E_m}[(r_p/r)^3 - 1] \quad [37]$$

The elastic work per unit volume of an element located at distance r is

$$\omega^e(r) = \frac{1}{2}[\sigma_r(e_r - e_r^p - \alpha_m \cdot \Delta T) + 2\sigma_\theta(e_\theta - e_\theta^p - \alpha_m \cdot \Delta T)]$$
$$= \frac{6(1-2\nu_m)\sigma_y^2}{E_m}[\ln(r/a)]^2 + \frac{2(1-2\nu_m)(2\sigma_y - 3P_1)\sigma_y \ln(r/a)}{E_m}$$
$$- \frac{1}{E_m}\left[2(1-2\nu_m)\sigma_y P_1 - (1-\nu_m)\sigma_y^2 - \frac{3}{2}(1-2\nu_m)P_1^2\right] \quad [38]$$

Similarly, the elastic strain energy per unit volume stored outside the plastic zone is

$$\omega^{out}(r) = \frac{(1+\nu_m)^2\sigma_y^2}{6(1-2\nu_m)E_m}(r_p/b)^6 + \frac{(1+\nu_m)\sigma_y^2}{3E_m}(r_p/r)^6 \quad [39]$$

D. *Relationship between 2b and Volume Fraction, ϕ*

It is now necessary to find a relationship between the ceramic volume fraction, ϕ, and interparticle distance, $2b$. For a polydispersed system of particles, an accurate relationship is difficult to obtain. However, when all of the particles are assumed to have the same radius, a, it can be shown[12] that for randomly distributed particles, the average half distance, b, between two neighboring particles is

$$b = a + \frac{a \cdot \exp(8\phi)}{6\phi^{1/3}} \int_{8\phi}^{\infty} x^{-2/3} e^{-x}\, dx \quad [40]$$

Equation [40] is known to be accurate when the volume fraction, ϕ, approaches zero. Thus, the maximum ϕ value in this study is limited to 0.1. Table I lists some b/a ratios obtained with Eq. [40].

III. EXPERIMENTAL PROCEDURES

Composite materials of the prealloyed 2024 Al powders and ceramic particles were fabricated *via* hot pressing and hot rolling. The average sizes of the ceramic particles are listed in Table II. The ceramic materials were blended with prealloyed 2024 Al powders, vacuum hot pressed at 495 °C for 2 hours as 50-mm-diameter, 13-mm-long disks under a pressure of 3000 psi. The hot-pressed samples were then wrapped with thin Al foils in order to prevent any reaction between the composites and the copper tube during heating and hot rolling, encapsulated with copper tube under vacuum, heat-treated to 515 °C (above the solidus temperature), and hot rolled to 2-mm-thick sheets in five passes. Three different volume percents of ceramic particles were considered: 0, 2, and 10 pct. The 0 vol pct sample served as a control.

Table I. Some Values of Interparticle Spacing (Equation [40])

ϕ	b/a
0.001	4.497
0.002	3.591
0.005	2.686
0.010	2.183
0.020	1.802
0.050	1.450
0.100	1.275
0.200	1.160
0.500	1.073

The samples were solutionized at 490 °C for 1 hour in a salt bath and subsequently water quenched.

Dislocation structures were analyzed for both the composites and the control alloy using a PHILIPS* EM301 transmission electron microscope operating at 100 kV. Transmission electron microscopy samples were chemically thinned with a 10 pct NaOH, 90 pct H_2O solution to a thickness of less than 150 μm to prevent introduction of dislocations during a thinning process. Then, 3-mm-diameter disks were prepared and jet polished with a 30 pct nitric acid, 70 pct methanol solution using a potential of 35 V at a temperature of about −30 °C. The dislocation density, ρ, was determined from a micrograph using the formula, $\rho = 2N/Lt$, where N is the number of dislocation intersections with a grid line of length, L, divided by the magnification, and t is the thickness of the sample.[13] It should be noted that the dislocation density thus obtained can be lower than an actual value because of a low operating power of the EM301 microscope. The thin foil thickness was measured using a JEOL-100CX transmission electron microscope operating at 120 kV. Without liquid N_2 cold stage, the foil surface was contaminated in 5 to 10 minutes by the focused electron beam. The thickness was measured from a micrograph showing the projected length between the contaminated spots of upper and lower foil surfaces using $t = d/\sin\theta$, where d is the projected length and θ is the primary tilting angle, equal to ~40 deg in this study. The thin foil thickness was measured as a function of distance from the Al/ceramic interface. Each thickness value at each point was incorporated for measurements. A circular test line was used to eliminate the effect of any preferred orientation of a dislocation structure, and the length of a grid line was 76 cm.

*PHILIPS is a trademark of Philips Instruments Corporation, Mahwah, NJ.

Table II. Average Size and Volume Fraction of Materials

Matrix	Ceramic	Vol Pct
2024 Al	SiC (22 μm)	0, 2, 10
2024 Al	SiC (14 μm)	0, 2, 10
2024 Al	SiC (5 μm)	0, 2, 10
2024 Al	TiC (30 μm)	0, 2, 10

IV. RESULTS

A. *Stress and Strain Energy Distribution in Composites*

Material parameters used for the calculation are given in Table III. Figure 2 presents the normalized stress with respect to the yield stress of the matrix as a function of the normalized distance from the ceramic center in the Al/SiC system. The value of unity for r/a corresponds to the matrix/ceramic interface. The stress distributions in the purely elastic state and in the elastoplastic state are displayed for $\phi = 0$ (a single particle) and $\phi = 0.003$, respectively. Matrix stress components, σ_r and σ_θ, are relatively short-ranged, decaying effectively to zero at approximately $r = 3a$. It is noted that the difference in the stress state between the two cases is significant within the ceramic particle as well as in the plastic zone but not in the elastic region of the matrix. Inside the plastic zone, the tangential stress is quite different, with the sign being reversed from its counterpart of the pure elastic case. The plastic zone size is seen to increase with increasing ceramic volume fraction.

In Figure 3, the normalized strain energy density is plotted as a function of the normalized radial distance for the three different volume fractions. The strain energies were normalized with respect to the plastic strain energy per unit volume for $\phi = 0$ at $r = a$. When the plastic zones overlapped each other, the plastic strain energy densities were calculated through superposition. Note that the plastic strain energy density decreases inversely with r^3 (Eq. [36]) and is seen to increase with volume fraction of ceramic. In the case of $\phi = 0$, the theoretical plastic zone size, r_p, is found to be $2.41a$ for Al/SiC composites and $2.27a$ for Al/TiC composites. The theoretical plastic zone size, r_p, is found not to increase rapidly with an increase in ϕ, but plastic zones start to overlap each other at $\phi = 0.007$ for Al/SiC composites as $r_p \cong b$ at this volume fraction.

B. *Dislocation Generation*

Dislocation density gradient showing a higher density near the Al/SiC interfaces is observed in the as-quenched $\phi = 0.02$ and 0.1 Al/SiC composites (Figures 4 and 5). Line, helical, and loop-type dislocations can be seen in the matrix. For Al/SiC composites with $\phi = 0.02$, the dislocations near the Al/SiC interface are generally in tangled arrangements, whereas dislocations away from the SiC particle are not, as shown in Figure 4. As the SiC volume fraction increased, dislocation density seemed to increase, and the dislocations also occupied a wider area (Figure 5). As expected, more dislocations were generated at a corner of a SiC particle, where a higher stress was concentrated during cooling (arrow marked).

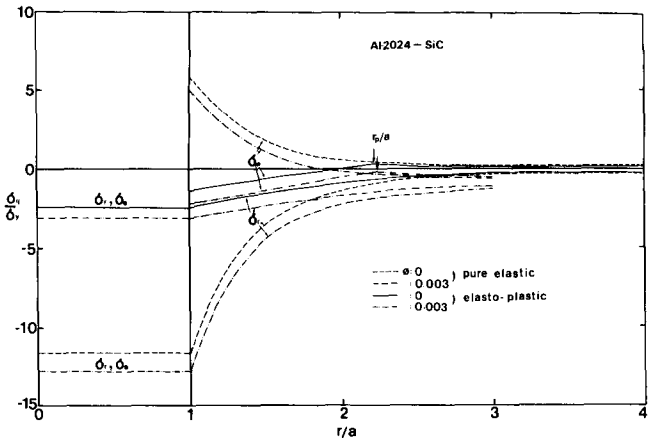

Fig. 2—The stress distribution in the purely elastic state and in the elastoplastic state in Al/SiC composites. The matrix/ceramic interface locates at $r/a = 1$. The volume fraction effects are displayed for $\phi = 0.003$. The stresses are normalized with respect to σ_y.

Similar to the findings of Vogelsang *et al.*,[1] the intensity of dislocation generation at the Al/ceramic interface is related to the size and shape of SiC particles. Figure 6 reveals a low intensity for dislocation generation in the vicinity of a small SiC particle with diameter

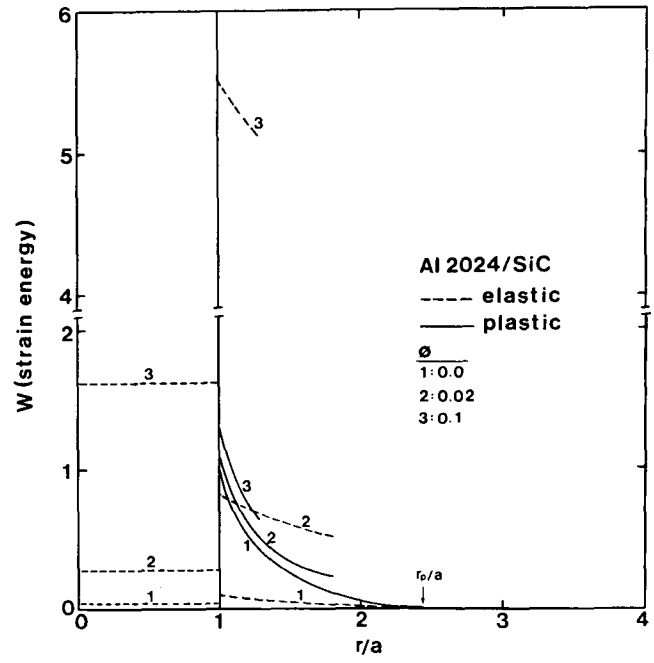

Fig. 3—The strain energy distribution in the elastoplastic state in Al/SiC composites. The strain energies are normalized with respect to the plastic strain energy per unit volume at $r = a$ for the case of $\phi = 0$. The volume fraction effects are displayed for $\phi = 0.02$ and 0.1.

Table III. Material Parameters

Material	Yield Strength (MPa)	Elastic Modulus (GPa)	Poisson's Ratio	Thermal Expansion Coefficient (K^{-1})	Thermal Misfit Strain
2024 Al	76	73	1/3	24×10^{-6}	—
SiC	—	510	0.19	4.4×10^{-6}	0.0091
TiC	—	310	0.19	7.4×10^{-6}	0.0077

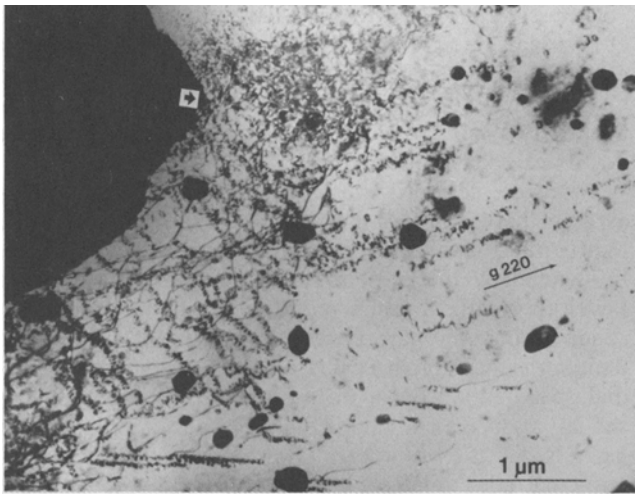

Fig. 4—Dislocation generation near an Al/SiC interface for $\phi = 0.02$. The ceramic particle diameter is 7.4 μm. Note the small intermetallic compounds associated with a 2024 Al alloy.

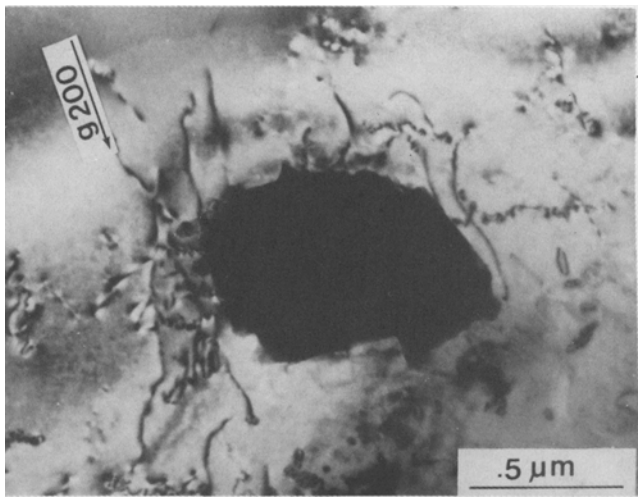

Fig. 6—Dislocation generation in the vicinity of a small SiC particle for $\phi = 0.02$. The ceramic diameter is 0.8 μm.

0.8 μm. No significant dislocation density gradient is observable in this case. As the particle diameter increases (to ~7 μm in Figure 4 and ~17 μm in Figure 7), the intensity of dislocation generation increases significantly. In comparing the present result with those of Vogelsang *et al.*[1] and Arsenault and Fisher,[2] an interesting observation is that much more helical dislocations seemed to be generated in the 2024 Al matrix than in the 1100 Al or 6061 Al matrices. No detailed studies were performed to find the cause of this morphological difference, but one possible reason is that for the present 2024 Al alloy, the water quenching right after a solutionizing treatment should have produced quenched-in vacancies or vacancy loops, which might have helped to nucleate helical dislocations. The 1100 and 6061 Al alloy samples, however, were furnace- or air-cooled after annealing.[1,2]

Figure 8 shows dislocation generation in a $\phi = 0.02$ Al/TiC composite, in which the particle size is 16.2 μm. As compared with an Al/SiC composite in Figures 4 or 7, the dislocation density is found to be significantly less. This decrease can be attributed to smaller differences in both the thermal expansion coefficient and elastic modulus between Al and TiC (Table III).

Dislocation density is plotted as a function of a normalized distance from the Al/ceramic interface in Figure 9. Also included are theoretical density curves obtained with the plastic strain energy term of Eq. [37]. Theoretical dislocation density is approximated as $\rho_t \cong \rho_0 + f\omega^p(r)/(0.5\mu\mathbf{b}^2)$, where ρ_0 is the dislocation density in the control alloy ($\sim 5 \times 10^8$ cm^{-2}), μ is the matrix shear modulus, $\mathbf{b}$ is the Burgers vector, and f is a partitioning parameter which reflects the fractional amount of the plastic strain energy stored as dislocations. In plastic deformation, part of the plastic work is dissipated, and defects other than dislocations are produced. However, in the absence of our detailed knowledge on the partitioning of a plastic work, the parameter, f, was arbitrarily taken as 0.5 in Figure 9. Each set of the experimental data in Figure 9 represents density measurements from a TEM micrograph.

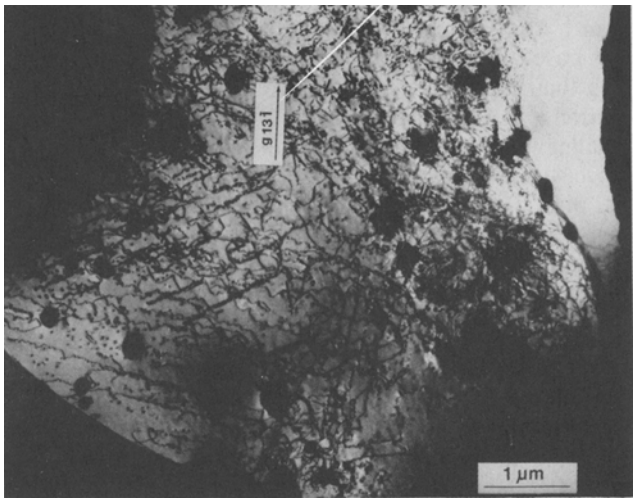

Fig. 5—Dislocation generation near an Al/SiC interface for $\phi = 0.1$. The ceramic particle diameter is 7.4 μm.

V. DISCUSSION

Residual stress is an inherent characteristic for composite materials. When composites are cooled to the room

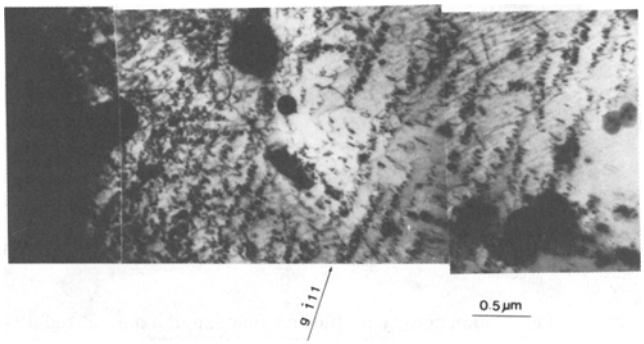

Fig. 7—Dislocation generation in the vicinity of a large SiC particle for $\phi = 0.02$. The ceramic diameter is 17.4 μm.

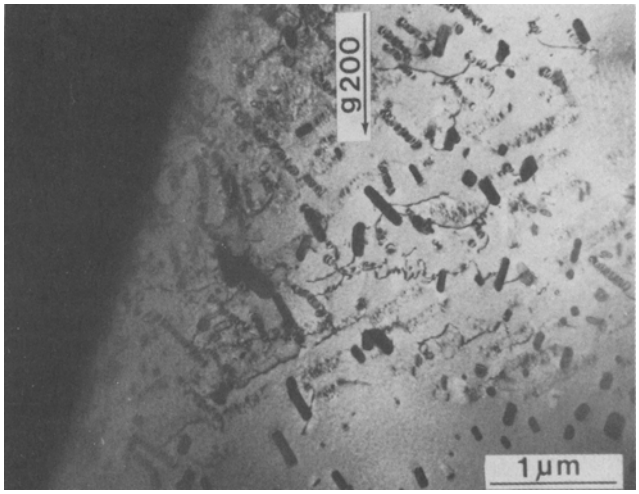

Fig. 8—Dislocation generation in an Al/TiC composite with $\phi = 0.02$. The particle size is 16.2 μm.

temperature from the fabrication or solutionizing temperature, residual stresses are introduced into the composites due to a mismatch in thermal expansion coefficient between the matrix and ceramic phases. Ledbetter and Austin[15] measured the average residual stress for 6061 Al composites containing 30 vol pct SiC particles *via* X-ray diffraction analysis. A hydrostatic tensile stress was found in the aluminum matrix, while a hydrostatic compressive stress was found in the SiC particles. Arsenault and Taya[16] observed that the tensile yield stress was greater than the compressive yield stress by ~13 MPa for 6061 Al composites containing 20 vol pct spherical SiC particles, suggesting a possibility that a compressive residual stress existed in the matrix. Though at first glance the two measurements appear to contradict each other, we should note that residual stresses depend on several factors, such as the volume fraction and distribution of ceramic particles[17] and also possibly on the details of heat transfer during cooling.

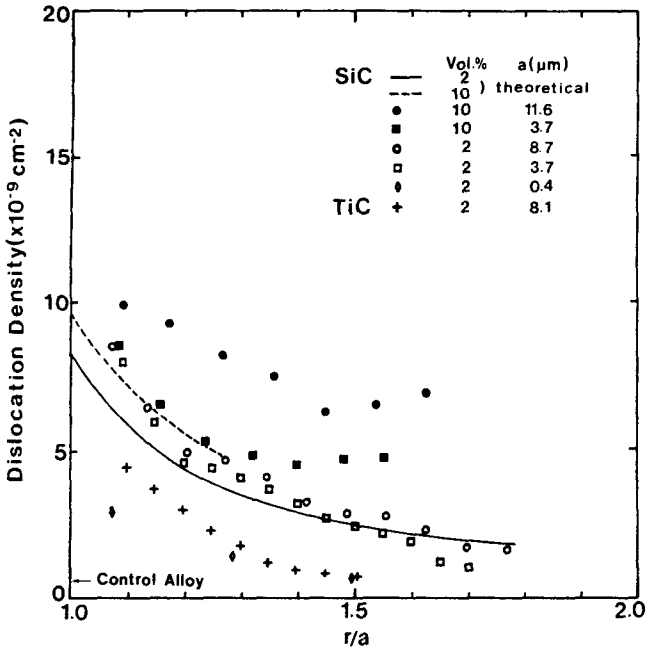

Fig. 9—Dislocation density profile as a function of a normalized distance from an Al/ceramic interface. The theoretically calculated densities are displayed for $\phi = 0.02$ and 0.1 Al/SiC composites.

When the ceramic volume fraction is small, we may assume that each ceramic particle is surrounded by the matrix phase, and the average interparticle spacing is not influenced by the presence of a ceramic phase with a lower thermal expansion coefficient. In this situation, spherical ceramic particles are in a hydrostatic state and their surrounding matrix phase suffers a compressive radial stress state. Thus, on the average, the composites should produce a compressive residual stress. On the other hand, when the volume fraction is so high that the ceramic particles touch each other, the ductile matrix phase should be considered enclosed by the ceramic phase. In this case, the ceramic particles are still in a compressive stress state, as is the matrix in the proximity of the ceramic particles. However, the majority of the matrix phase with a higher thermal expansion coefficient should undergo shrinking on cooling, resulting in a tensile residual stress. The actual conditions of composites may fall between the two extreme cases. In light of this discussion, we note that the boundary conditions (Eqs. [8a] through [8c]) employed in the present model are based on the approximation of a small volume fraction, ϕ, and thus the model's prediction should yield an overestimation for the plastic strain energy density (and the dislocation density) at a high ϕ. In this regard, other boundary conditions reflecting the volume fraction of ceramic particles are certainly desirable as a future study.

According to the early studies on the inclusion size-dependent yield stress,[4,7,8] the effective yield stress for dislocation generation should approach the macroscopic yield stress of the matrix phase if the ceramic particle size becomes of the order of a few microns and the ceramic-matrix interface is incoherent. Therefore, the dislocation density gradient showing a higher density near the Al/ceramic interface should be observed when the ceramic particle size is over a few microns (Figures 4, 5, and 7). No significant dislocation density gradient, however, is observed when the particle diameter is less than 1 μm (Figure 6). Several reasons can be offered for this case. The stress due to the thermal misfit could be less than the effective yield stress for dislocation generation.[4,8] Alternatively, in case the plastic zone size is smaller than the characteristic dislocation punching distance, the dislocation generated first would possibly reach the plastic zone front, thus limiting the further dislocation generation through the influence of the back stress.[7] It should be also noted that a stable, polygonized dislocation structure can be developed around a submicron particle, as nicely demonstrated in the high-voltage electron microscopy work of Vogelsang *et al.*[1]

Although Figure 9 shows a fair agreement, at least qualitatively, between the measured and calculated dislocation density, we note that the calculated dislocation density depends on the partitioning parameter, f, that appeared in the formula $\rho_t \cong \rho_0 + f\omega^p(r)/(0.5\mu\mathbf{b}^2)$. As mentioned before, some of a plastic work is dissipated

as heat and some is spent for producing various defects. One can estimate the value of f from a macroscopic tensile or compression test. However, it should be noted that the present microscopic situation is quite different from a macroscopic case; thus, the use of such an experimental value for f is not necessarily valid. In view of this uncertainty of f, further studies are necessary for a useful application of the present micromechanics analysis. As an alternative, an effective plastic strain can be used for estimating dislocation densities, but it requires a mean free path for dislocations, which is again a quantity as ambiguous as heat dissipation.[1] When two ceramic particles with a thermal misfit strain approach each other, there arises an additional stress field due to the difference in elastic constants between the matrix and ceramic phase.[14,18] However, the strength of this inhomogeneity-induced stress is proportional to r^{-6} (as compared with the r^{-3} terms of Eqs. [12a] and [12b]) and was neglected in the present analysis.

No *in situ* TEM work was performed for the present 2024 Al composites, but the work of Vogelsang *et al.*[1] on 6061 Al/SiC composites found that most of the dislocations were annealed out at 507 °C. Thus, it appears quite reasonable to use the solutionizing temperature of 490 °C as the reference temperature at which all of the displacements were assumed to disappear. The plastic relaxation of the matrix surrounding a thermal misfitting ceramic particle can lead to substantial changes in the associated stress field and strain energy. This results in elastic and plastic strain energy gradients around the ceramic particles. Aluminum alloy matrix/ceramic composites are somewhat unique since the properties of the aluminum matrix itself can be modified and varied significantly through the precipitation process. The drastic change in the stress field surrounding the ceramic particles, therefore, can affect diffusion, kinetics of precipitate nucleation and growth, coherency state, *etc.* It would be of great value to understand the effects of the plastic relaxation on the precipitation kinetics.

VI. CONCLUSIONS

From the experimental data and the theoretical model, the following conclusions were made:

1. A theoretical model for the plastic relaxation of thermal misfit stress in composites was developed such that the model incorporates the volume fraction of spherical ceramic particles. Its prediction of the plastic strain energy gradient around the ceramic particles was found to be in a fair agreement with the observed dislocation density gradient.
2. As the volume fraction of ceramic particles increased, the dislocation density increased, and the dislocation structure became more tangled due to the interaction between thermal misfit stress fields.
3. The intensity of dislocation generation due to the different thermal contractions seemed to be strongly influenced by the ceramic particle size and also by the difference in elastic modulus between the ceramic and matrix.

NOMENCLATURE

a	spherical ceramic radius
b	half of interparticle spacing
σ_r	radial stress component
σ_θ	tangential stress component
σ_e	equivalent stress
σ_y	yield stress of the matrix phase
e_r	radial strain component
e_θ	tangential strain component
e_r^p	radial plastic strain component
e_θ^p	tangential plastic strain component
E	elastic modulus
μ	shear modulus
ν	Poisson's ratio
α	coefficient of thermal expansion
T	temperature
ΔT	temperature of measurement − solutionizing temperature
u	radial displacement
r_p	plastic zone radius
P_1	internal pressure
P_2	external pressure
ϕ	volume fraction of the ceramic

Subscripts

m	matrix
c	ceramic

ACKNOWLEDGMENTS

The authors are grateful to Professor R.J. Arsenault for his critical reading of the manuscript and many constructive suggestions. They also wish to acknowledge the financial support provided by ALCOA (contributions of CTK and MRP) and by the Division of Materials Research of the National Science Foundation under Grant No. DMR-8508720 (contributions of JKL and MRP).

REFERENCES

1. M. Vogelsang, R.J. Arsenault, and R.M. Fisher: *Metall. Trans. A*, 1986, vol. 17A, pp. 379-89.
2. R.J. Arsenault and R.M. Fisher: *Scripta Metall.*, 1983, vol. 17, pp. 67-71.
3. K.K. Chawla and M. Metzger: *J. Mater. Sci.*, 1972, vol. 7, pp. 34-39.
4. J.K. Lee, Y.Y. Earmme, H.I. Aaronson, and K.C. Russell: *Metall. Trans. A*, 1980, vol. 11A, pp. 1837-47.
5. C.A. Hoffman: *J. Eng. Mater. Technol.*, 1973, vol. 95, pp. 55-62.
6. Y.Y. Earmme, W.C. Johnson, and J.K. Lee: *Metall. Trans. A*, 1981, vol. 12A, pp. 1521-30.
7. W.C. Johnson and J.K. Lee: *Acta Metall.*, 1983, vol. 31, pp. 1033-45.
8. M.F. Ashby and L. Johnson: *Phil. Mag.*, 1969, vol. 20, pp. 1009-22.
9. R. Hill: *The Mathematical Theory of Plasticity*, Oxford University Press, London, 1950, p. 97.
10. A. Mendelson: *Plasticity—Theory and Applications*, MacMillan Publishing Company, New York, NY, 1968, p. 135.
11. G.E. Dieter: *Mechanical Metallurgy*, McGraw-Hill, New York, NY, 1961, p. 58.
12. A.J. Ardell: *Acta Metall.*, 1972, vol. 20, pp. 61-71.

13. P.B. Hirsch, A. Howie, R.B. Nicholson, D.W. Whelan, and D.W. Pashley: *Electron Microscopy of Thin Crystals*, 2nd ed., Krieger, New York, NY, 1977, p. 422.
14. J.D. Eshelby: *Proc. R. Soc.*, 1957, vol. 241A, pp. 376-96.
15. H.M. Ledbetter and M.W. Austin: *Mater. Sci. Eng.*, 1987, vol. 89, pp. 53-61.
16. R.J. Arsenault and M. Taya: *Acta Metall.*, 1987, vol. 35, pp. 651-59.
17. N.K. Asamoach and W.G. Wood: *J. Strain Anal.*, 1970, vol. 5, pp. 88-97.
18. W.C. Johnson and J.K. Lee: *Metall. Trans. A*, 1979, vol. 10A, pp. 1141-49.